Electronic Supplementary Information

Polymorphism of Low Dimensional Boron Nanomaterials Driven by Electrostatic Gating: A Computational Discovery

Yalong Jiao[1,4,*], Fengxian Ma[1,3], Jinxing Gu,[2] Zhongfang Chen,[2,*] Aijun Du[1,*]

[1] School of Physics and Chemistry and Centre for Materials Science, Queensland University of Technology, 2 George Street, Brisbane, QLD 4000 Australia.

[2] Department of Chemistry, University of Puerto Rico, Rio Piedras Campus, San Juan, PR 00931, United States

[3] Department of Physics, Hebei Normal University, Shijiazhuang 050024, China

[4] Theoretische Chemie, Technische Universität Dresden, Dresden 01062, Germany

***E-mail:** yalong.jiao@hdr.qut.edu.au;
zhongfangchen@gmail.com;
aijun.du@qut.edu.au

Details for the formation energy and interlayer binding energy computations

The formation energy E_f of boron ribbon/sheet on the Ca_2N layer is defined with the following equation:

$$E_f = 1/n(E_{tot} - E_{Ca2n} - nE_B)$$

where E_{tot} and E_{Ca2n} represent the total energy of relaxed boron ribbon/Ca_2N system, and pristine Ca_2N layer, respectively. E_b is the energy of an isolated spin-polarized boron atom and n is the number of boron atoms in the simulation box.

The interlayer binding energy was evaluated based on the equation:

$$E_b = 1/n(E_{tot} - E_{Ca2n} - E_{Bs})$$

Here E_{tot}, E_{Ca2n} and E_{Bs} are the total energies of the relaxed boron ribbon/Ca_2N system, pristine Ca_2N layer and boron ribbon or sheet, respectively. The calculated interlayer binding energy (E_b) for ribbon + Ca_2N is -0.605 eV/atom, which is lower than the boron sheet + Ca_2N system (-0.424 eV/atom). The calculated E_b for β_3 boron sheet/Ca_2N complex is the highest among the three systems with a value of -0.207 eV/atom.

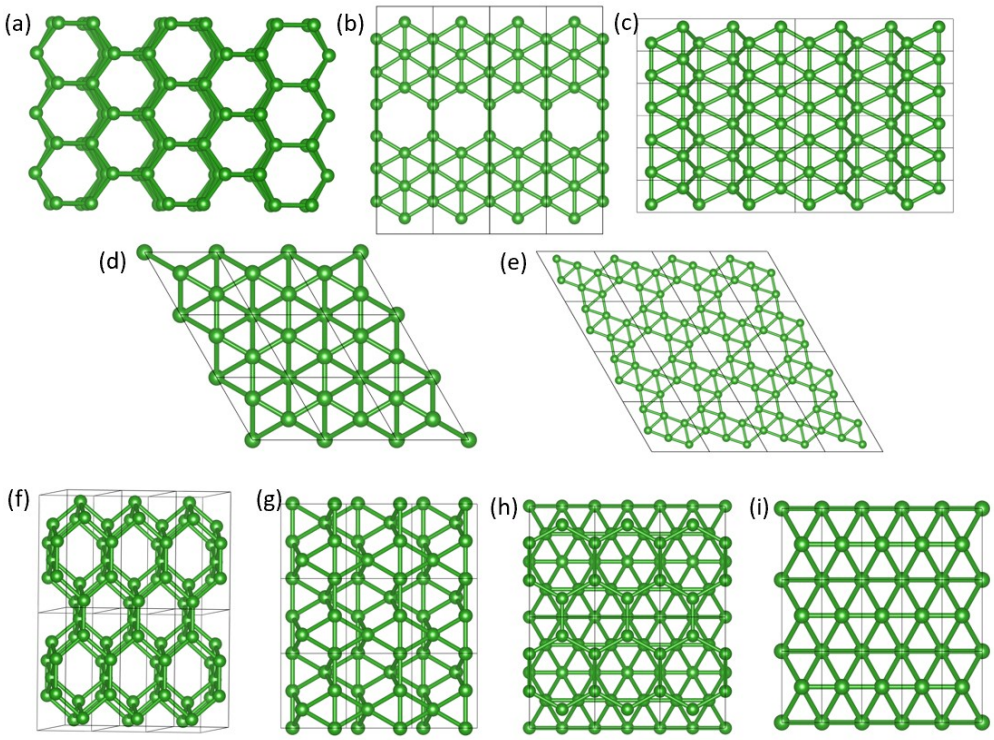

Figure S1. Top view of various low-lying energy 2D boron structures at the charge-neutral state. The structure search was performed with a unit cell of 6 atoms.

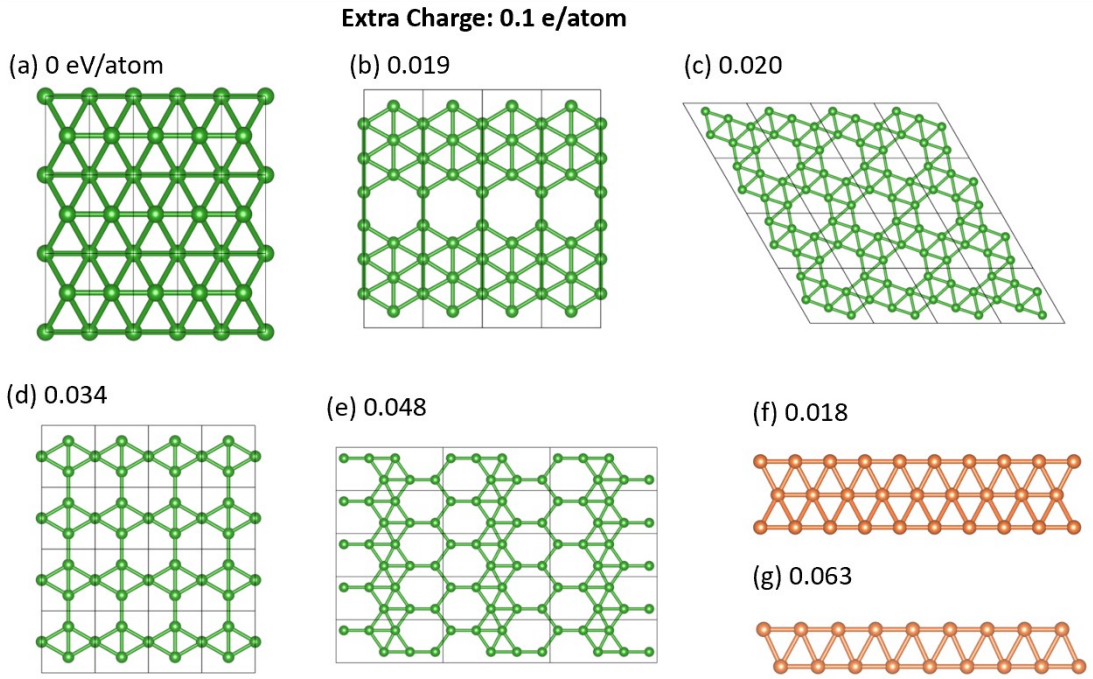

Figure S2. Top view and energies of various low-lying energy boron structures with the electron injection of 0.1 e/atom. The 1D and 2D boron configurations are distinguished by orange and green balls, respectively.

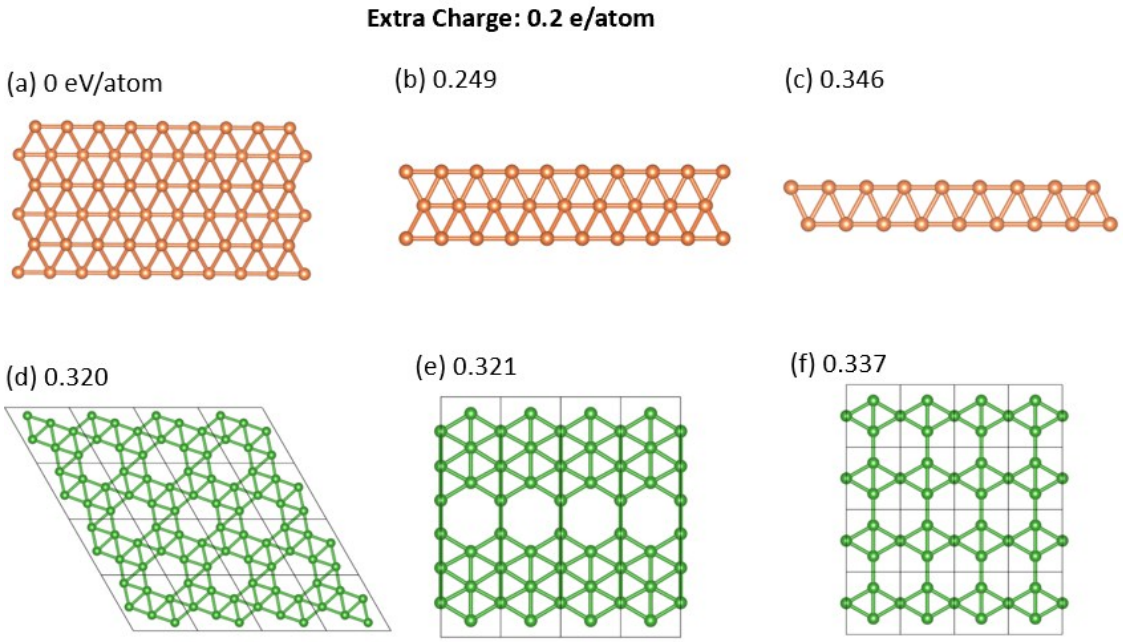

Figure S3. Top view and energies of various low-lying energy boron structures with the electron injection of 0.2 e/atom. The 1D and 2D boron configurations are distinguished by orange and green balls, respectively.

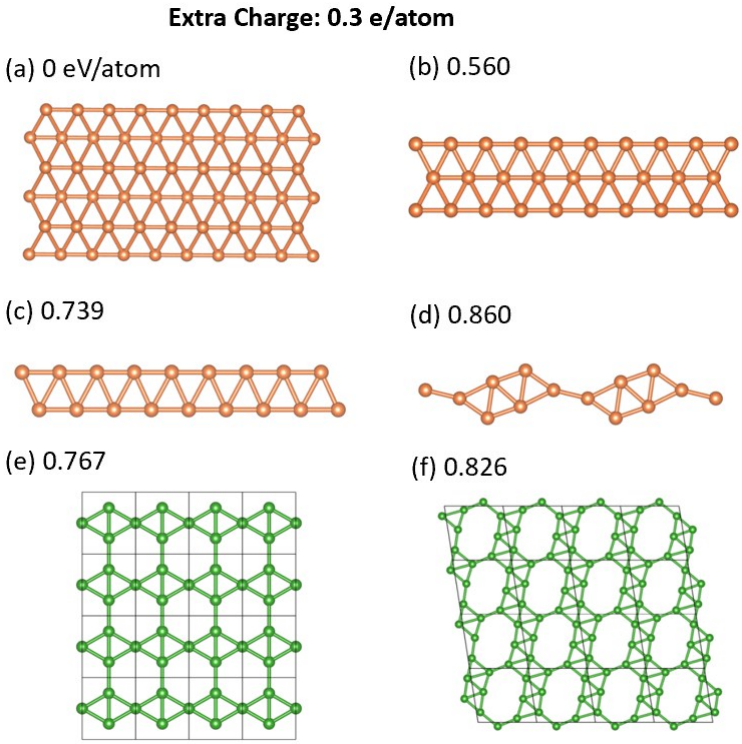

Figure S4. Top view and energies of various low-lying energy boron structures with the electron injection of 0.3 e/atom. The 1D and 2D boron configurations are distinguished by orange and green balls, respectively.

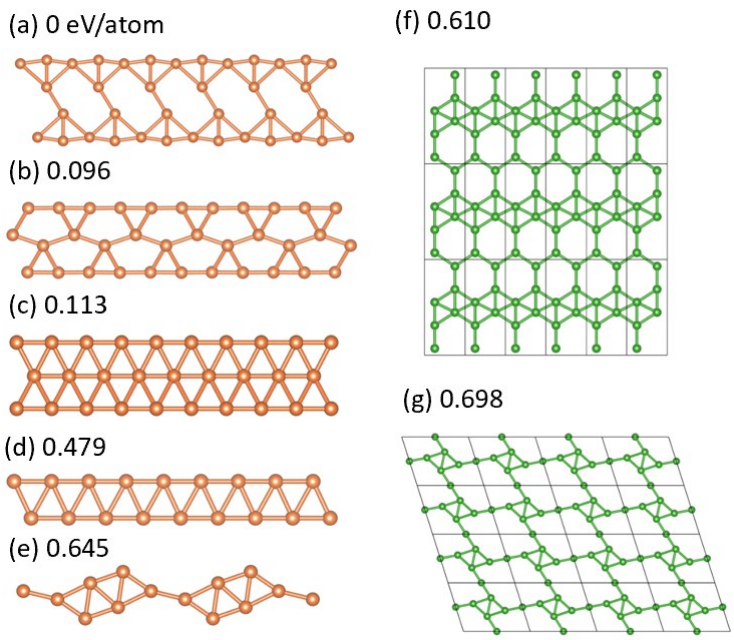

Figure S5. Top view and energies of various low-lying energy boron structures with the electron injection of 0.5 e/atom. The 1D and 2D boron configurations are distinguished by orange and green balls, respectively.

Note that the boron ribbon mixed with triangle & pentagon (Figure S5b) only exists under a certain charge density level, and it undergoes a phase transition to the FBR (Figure S5c) at the charge neutrality. Similarly, the truss-like ribbon (Figure S5e) transfers to TAR phase (Figure S5d) at the neutral state. The four-atom wide boron ribbon (Fig. S5a) transfers to FAR_{hex} phase (Fig. S12) at the neutral state.

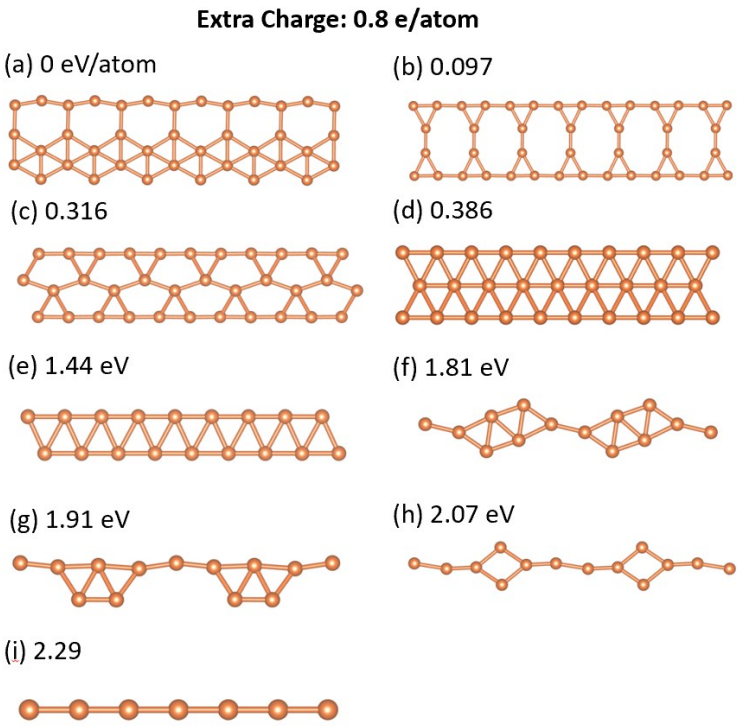

Figure S6. Top view and energies of various low-lying energy boron structures with the electron injection of 0.8 e/atom.

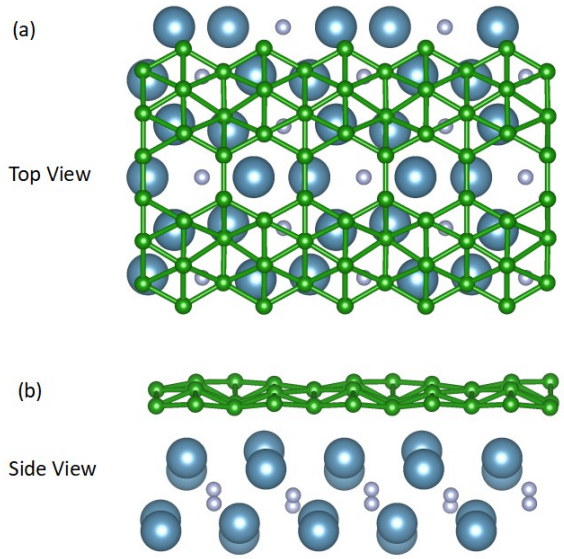

Figure S7. Top and side views of the β_3 boron sheet/Ca_2N complex.

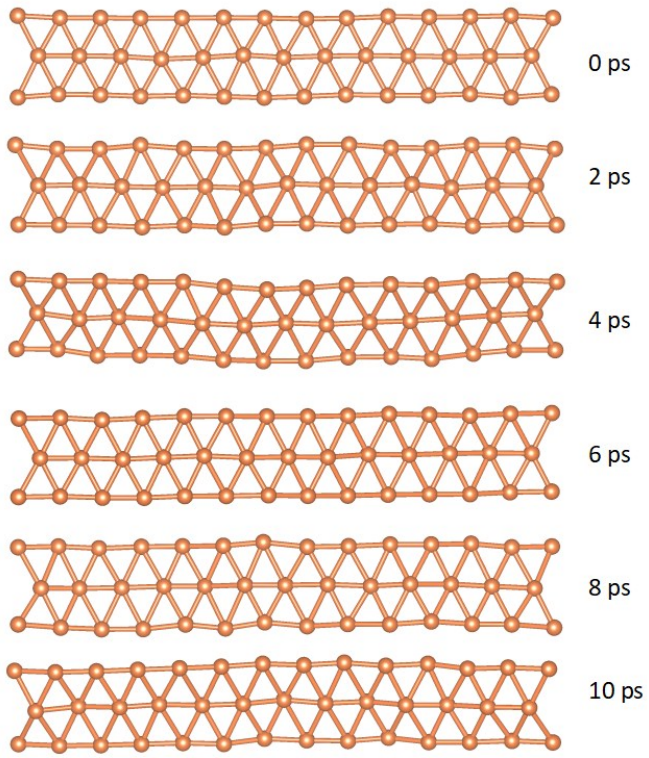

Figure S8. Snapshots from AIMD simulation of the FBR at 300 K.

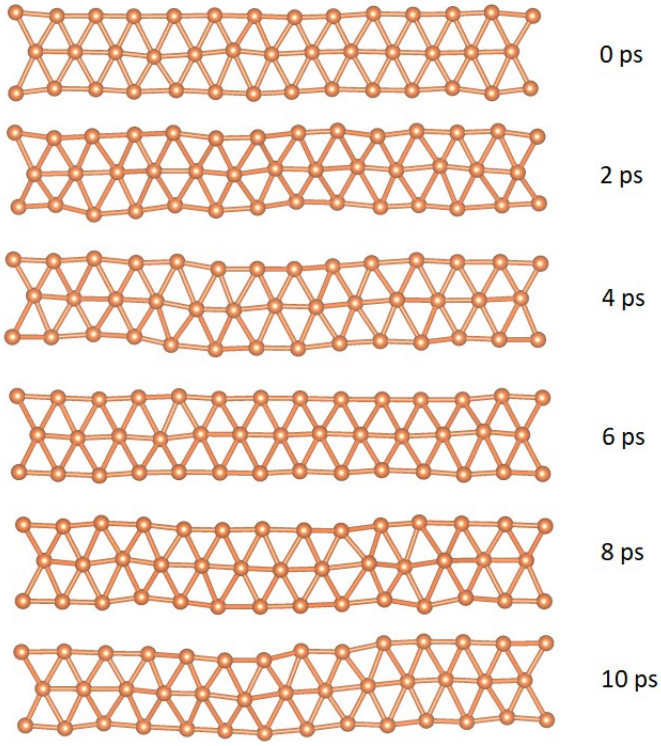

Figure S9. Snapshots from AIMD simulation of the FBR at 800 K.

The thermal stability of FBR was examined by performing the *ab initio* molecular dynamics (AIMD) simulations in the NVT ensemble. AIMD was performed with a Nose-Hoover thermostat at 300 K and 800 K, respectively. After heating up and

maintained at the targeted temperature for 10 ps, the structural disruption for this ribbon cannot be observed (see Figure S8 - Figure S9).

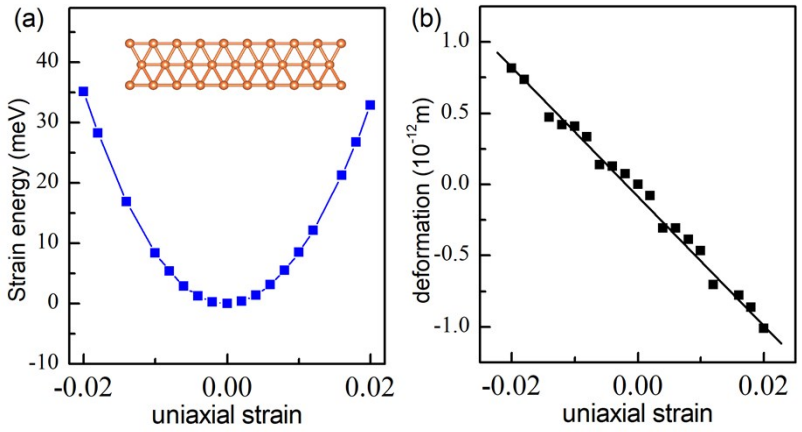

Figure S10. (a) Strain-energy and (b) strain-deformation vs. uniaxial strain for borophene-like ribbon (FBR).

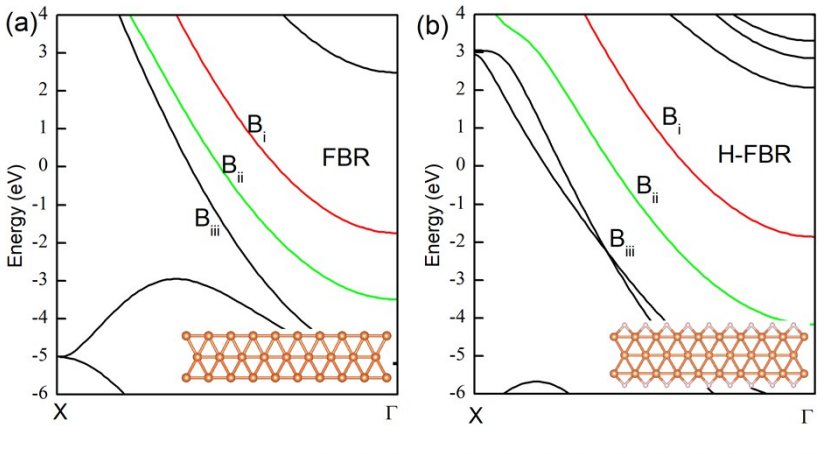

Figure S11. The band structure of FBR and hydrogenated FBR on GGA-PBE level.

The dangling bonds may exist at the edges of ribbons. Therefore, we used the hydrogen atoms to saturate the dangling bonds and calculated the electronic property of the hydrogenated FBR (H-FBR) in Figure S11. At the Fermi level, we find the bands (B_i and B_{ii}) of H-FBR have a slight difference compared with those in FBR. But the hydrogen atoms in H-FBR introduce an extra band crossing (B_{iii}) which does not exist in pure FBR.

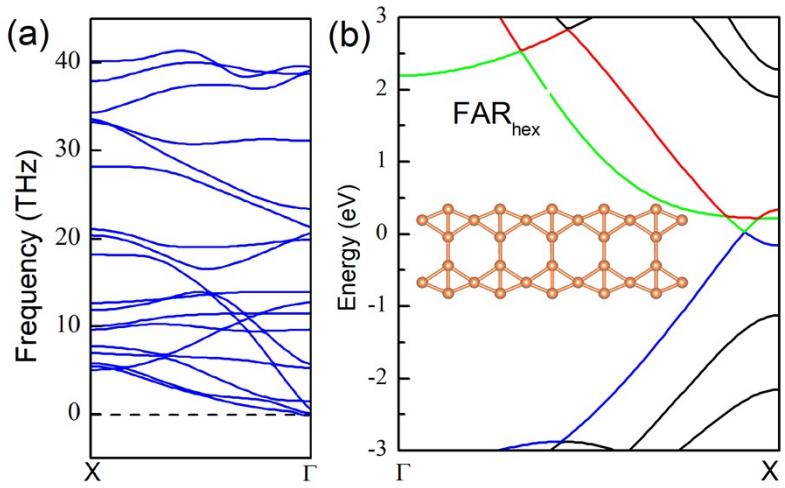

Figure S12. (a) Phonon band dispersion and (b) band structure of FAR_{hex} calculated by HSE06 method. The Femi level is set to zero.

A four-atom wide ribbon with hexagonal holes FAR_{hex} as shown in the inset of Figure S12b. In Figure S12b, the valence band maximum and conduction band minimum of FAR_{hex} meet at the Fermi level, leading to a linear band dispersion. Note that these touching points are Dirac points, which indicates the ribbon possesses ultra-high electron transport and massless Dirac fermions. No negative modes can be found in the phonon spectrum, demonstrating it is dynamically stable (Fig. S12a). To the best of our knowledge, this is the first example of the Dirac cone feature discovered in 1D boron structures.